Iraqi Journal of Physics, 2026
https://doi.org/10.30723/ijp.v24i2.1517

Vol.24, No.2, PP.115-139
P-ISSN: 2070-4003
E-ISSN: 2664-5548

Analyzing Climatic and Environmental Trends in Iraq Using an Integrated GIS and Mann-Kendall Approach

Ayman Muwafaq Ahmed[1, 2*], Bushra Qassim AL-Abudi[1], and Alaa G. Khalaf[3]
[1]*Department of Astronomy and Space, College of Science, University of Baghdad, Baghdad, Iraq*
[2] *Department of Remote Sensing, Remote Sensing and Geophysics College, Alkarakh University of Science, Baghdad, Iraq*
[3]*Scientific Research Commission, Baghdad, Iraq*
[*]Corresponding author: aymenmuwafaq@kus.edu.iq

Abstract

This study investigates the spatial and temporal trends in selected climatic and environmental variables across various regions of Iraq from January to May during 2003 to 2024 using Geographic Information System (GIS) techniques and the Mann-Kendall trend test. The analysis focuses on five variables: air temperature, methane (CH_4), carbon monoxide (CO), carbon dioxide (CO_2), and the Soil-Adjusted Vegetation Index (SAVI). A comprehensive dataset was compiled by integrating satellite-based observations of climatic and environmental variables, MODIS remote sensing imagery for SAVI estimation, and observational air temperature data obtained from the Iraqi Meteorological Organization and Seismology. Temporal trends were assessed using the Mann-Kendall test, a non-parametric method for detecting monotonic changes, while the Theil-Sen slope estimator was used to quantify the rate of change over time. For spatial analysis, Iraq was classified into three climatic regions: northern, middle, and southern regions. This regional division facilitated clearer identification of spatial and seasonal variations in climate and environmental conditions. Results reveal strong regional contrasts. Middle and southern governorates experienced the highest warming rates, while northern regions showed weaker thermal changes. CH_4 increased significantly across all regions, whereas CO declined markedly. CO_2 exhibited a consistent upward trend nationwide. SAVI trends varied across regions: northern governorates showed positive vegetation responses, whereas southern and western regions showed stagnation or decline. Overall, middle and southern Iraq face the highest environmental stress due to accelerated warming, increasing greenhouse gas concentration, and reduced vegetation resilience, emphasizing the need for targeted adaptation measures and sustainable land management strategies.

Article Info.

Keywords:
Iraq, Soil-Adjusted Vegetation Index (SAVI), GIS, Climate, Methane.

Article history:
Received: Sep. 28, 2025
Revised: Jan. 18, 2026
Accepted:Feb. 01, 2026
Published:Jun. 01,2026

1. Introduction

In the context of accelerating global climate change, remote sensing has emerged as an effective method for analyzing environmental data and understanding climatic phenomena through quantitative surface classification. Within this context, the land surface temperatures of the Al-Hammar Marshes in Iraq for the years 1991, 2000, 2015, and 2017 were estimated using Landsat thermal bands processed in ENVI 5.1 to produce spatial temperature maps. The results demonstrated a steady increase in surface temperatures, rising from approximately 41.5 °C in 1991 to 47.9 °C in 2017, indicating a pronounced warming trend and underscoring the mounting climatic and environmental stress on the marshland ecosystem [1].

Iraq ranks among the top five countries most vulnerable to the impacts of climate change, particularly concerning water scarcity, food insecurity, and extreme temperatures. Climate studies spanning the period 1971–2020 indicate a marked increase in temperatures and a decrease in precipitation, especially in southern regions. Future projections under various emissions scenarios suggest that these trends are likely to intensify [2]. At the local scale, a study in Sulaymaniyah Governorate utilizing the Mann–Kendall test and Sen's slope estimator showed significant annual temperature increases at most meteorological stations. Rainfall trends were statistically

insignificant at the 95% confidence level, although slight localized fluctuations were observed [3]. Similarly, a 70-year analysis (1940–2010) in Sinjar District revealed a significant long-term decrease in annual rainfall, with monthly trends showing increases in October and April, while the rest of the months exhibited declining patterns [4]. An analysis of minimum, maximum, and mean temperatures across Mosul, Kirkuk, Baghdad, Rutba, and Basra over 1950–2021 revealed statistically significant upward trends in 99% of the months, with minimum temperatures increasing more sharply than maximums, particularly in Basra, highlighting the persistent impact of climate change on Iraq's temperature patterns [5]. Also, the analysis of precipitation data from twenty stations (1992–2010) using the Mann–Kendall test and Kendall–Tiehl estimator revealed significant downward trends in rainfall across most regions. The findings indicate an overall decline of about 3.5% in mean annual precipitation, emphasizing growing climatic stress and the progression toward drier conditions [6].

Analysis of air temperature records (Tmean, Tmax, and Tmin) from seven Iraqi stations (1941–2013) revealed notable temporal and spatial warming trends. Using linear regression and the Mann–Kendall test, the study identified stronger warming during summer months, accounting for nearly 89% of significant monthly trends. Results showed southern Iraq was most affected in Tmean and Tmax, while Tmin exhibited pronounced warming in northern and southern regions. Overall, inter-annual variations aligned with global warming patterns, with 2010 recorded as the hottest year across all stations [7].

Another study examined the relationship between climate variables and dust activity in the Tigris–Euphrates alluvial plain, one of the main dust storm zones in the Middle East. Using LSTM modeling and emission scenarios SSP2-4.5 and SSP5-8.5, the study projected increases in aerosol optical depth (AOD) by 10.5% and 15.2%, respectively, between 2021 and 2040. Key influencing factors included temperature, precipitation, and vegetation cover [8]. From 1980 to 2022, eleven thermal bioclimatic indicators were analyzed across Iraq using ERA5 reanalysis data. The Mann–Kendall test revealed significant warming trends, with the annual mean temperature (Bio1) rising between 0.28 and 0.48°C per decade, well above the global average. These changes were most pronounced in northern and eastern Iraq and included reduced diurnal temperature ranges and intensified summer heat [9].

Satellite-based observations from AIRS and OMI for the years 2017–2019 showed distinctive seasonal patterns in atmospheric pollutants such as carbon monoxide (CO), ozone (O_3), and nitrogen dioxide (NO_2). CO concentrations peaked in winter and spring, O_3 in late winter to late spring, and NO_2 levels were highest in densely populated areas, particularly Baghdad. The early months of the COVID-19 pandemic, particularly during curfews, were associated with temporary improvements in air quality [10]. On a broader temporal scale, data from seven Iraqi meteorological stations between 1972 and 2022 demonstrated clear temperature increases, reductions in solar radiation and wind speed, and declining rainfall trends. An increase in the frequency and severity of dust storms was also noted, further highlighting the profound impact of global warming on Iraq's climate system [11]. Another study analyzed the carbon dioxide intensity (CI) alongside total carbon dioxide (CO_2) emissions and per capita CO_2 emissions using data from CDIAC for the period 1971–2018. Results showed CI peaked at 7.188 kg/kg oil equivalent in 1971, decreased to 1.707 kg/kg in 1997, and then gradually rose to 3.63 kg/kg in the last decade [12]. Total CO_2 emissions strongly correlated with oil production, reaching 188.1 Mt in 2018, a 65.18% increase over the study period, and were inversely related to CI. Per capita CO_2 emissions fluctuated around 3.49 t/person, peaking at 4.99 t/person in 2013 [13].

Finally, a study analyzing tropospheric O_3 and associated atmospheric variables such as skin temperature, CO, and water vapor (H_2O) between 2003 and 2021 showed clear seasonal variations. Ozone concentrations peaked in spring, CO in winter, while skin temperature and water vapor were highest in summer. Spatially, pollutant levels were generally higher in northern Iraq. Trend analysis indicated rising trends in skin temperature and water vapor, a stable pattern for

ozone, and a significant decline in CO, offering essential insights for formulating effective air quality management strategies[14]. This study aims to investigate the spatiotemporal trends of selected climatic and environmental variables across Iraq during the period 2003–2024 using Geographic Information System (GIS) techniques and the Mann–Kendall trend test. The analysis focuses on air temperature, key atmospheric gases (CH_4, CO, and CO_2), as well as vegetation dynamics represented by the Soil-Adjusted Vegetation Index (SAVI). Spatial analysis was applied to identify regional variability, while temporal analysis was used to detect long-term trends. The selected study period was based on the availability of consistent satellite observations and ground-based data, allowing for a reliable assessment of recent climatic and environmental changes.

2. Study Area

Iraq covers an area of approximately 438,314 square kilometers and is located between latitudes 29.05° and 37.22° North, and longitudes 38.45° and 48.45° East (see Fig. 1). The country exhibits marked spatial variability in climate and environmental conditions due to its diverse topography and position at the junction of arid and semi-arid zones. Northern and northeastern mountainous areas experience cooler temperatures, higher and more evenly distributed precipitation, and distinct seasonal dynamics, while the middle and southern lowlands are characterized by higher temperatures, lower rainfall, and greater susceptibility to drought. These climatic and topographic gradients directly influence vegetation patterns, hydrological processes, and the distribution of atmospheric constituents, making them essential for spatially explicit environmental assessments. To capture these regional differences, Iraq was divided into three climatic zones: northern, middle, and southern, allowing a targeted analysis of temperature trends, greenhouse gas concentrations, and vegetation responses across distinct ecological and climatic contexts [15].

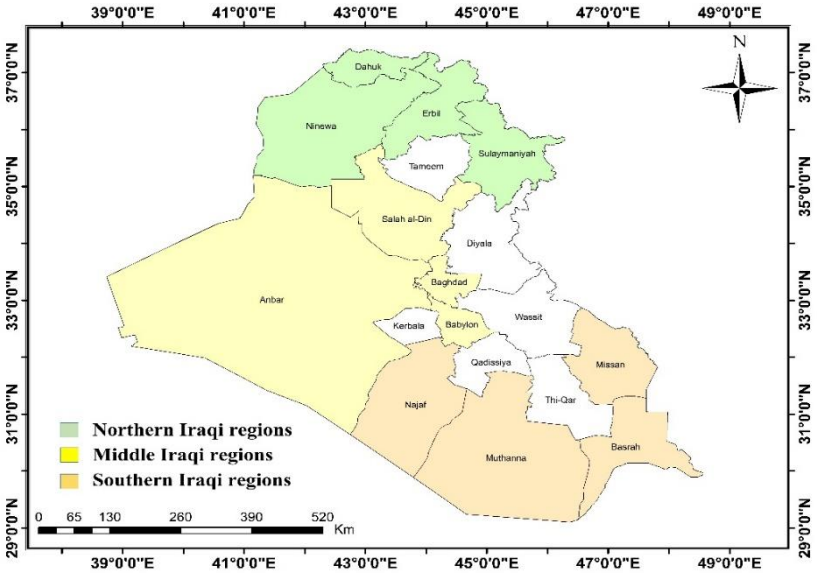

Figure 1: Map of Iraq.

3. Data and Methodology

3.1. Data Source

In this research, a set of data was used, such as monthly average air temperature data obtained from the Iraqi Meteorological Organization and Seismology. Methane (CH_4) and CO concentrations were sourced from the Atmospheric Infrared Sounder (AIRS), while CO_2 measurements for the period 2003 to 2014 were acquired from AIRS, and from 2015 to 2024, data

were obtained from the Orbiting Carbon Observatory-2 (OCO-2), Data were obtained from the NASA Goddard Earth Sciences Data and Information Services Center (GES DISC). Additionally, MODIS satellite imagery was used to calculate the monthly SAVI. Table 1 summarizes the climatic and environmental datasets used in the study, including sensor sources and their spatial and temporal resolutions. Also, ArcGIS 10.8 and SPSS software were used to analyze and output the results. Fig. 2 shows samples of the used data.

Table 1: The spatial and temporal resolutions of climatic and environmental datasets

Variable	Sensor / Mission	Spatial Resolution	Temporal Resolution
CH_4	AIRS / Aqua	~1° × 1° (~100 km)	Monthly
CO	AIRS / Aqua	~1° × 1° (~100 km)	Monthly
CO_2	AIRS / Aqua	~1° × 1° (~100 km)	Monthly
CO_2	OCO-2	~1.3 × 2.25 km	Monthly
Surface Reflectance	MODIS / Terra	500 m	8-day composite

3.2. Methodology

To effectively assess the spatiotemporal dynamics of climatic and environmental variables within a study area, it is essential to employ appropriate analytical tools and indices. Three fundamental components often used in such analyses are the Mann-Kendall Test, the SAVI, and Spatial Interpolation. Each plays a unique role in capturing and interpreting both temporal trends and spatial patterns in environmental data. This paper compiles monthly air temperature data from ground-based stations and applies spatial interpolation techniques to generate continuous surfaces covering the study area, which is Iraq. The resulting data were saved in (GeoTIFF) format. As indicated in Table 1, the spatial resolution of the datasets varied; therefore, a resampling procedure based on bilinear interpolation was applied to standardize all datasets to a common spatial resolution of 0.1° × 0.1°, ensuring consistency and suitability for regional-scale analysis. It should be noted that atmospheric composition variables (CH_4, CO, and CO_2) were extracted at the 500 hPa pressure level. The concentrations of CH_4 and CO are expressed in mole fraction units (mol mol^{-1}), while the CO_2 concentration is expressed in parts per million (ppm) . The 500 hPa level was chosen because near-surface atmospheric layers often suffer from data gaps and incomplete spatial coverage over the study area, particularly when using reanalysis and satellite-derived products. Data availability at lower pressure levels close to the Earth's surface does not provide continuous and homogeneous spatial coverage over Iraq. In contrast, the 500 hPa level offers more spatially complete, consistent, and reliable datasets, making it more suitable for spatiotemporal analysis at the regional scale.

In addition, other environmental variables were processed, including CH_4, CO, and CO_2). Furthermore, MODIS satellite imagery, composed of four tiles to ensure complete spatial coverage of Iraq, was used to calculate the monthly SAVI. Subsequently, climatic and environmental data were extracted for twelve selected Iraqi governorates and grouped into three regional clusters (north, middle, and south). Northern Iraq includes Duhok, Erbil, Sulaymaniyah, and Nineveh and is generally characterized by higher elevations, relatively cooler temperatures, and more favorable conditions for vegetation. Middle Iraq comprises Salah al-Din, Baghdad, Anbar, and Babil and represents a transitional zone with moderate climatic conditions and increasing exposure to anthropogenic and thermal stress. Southern Iraq includes Najaf, Maysan, Muthanna, and Basra and is characterized by low-lying terrain, arid to semi-arid climate, high temperatures, and limited precipitation, making it the most environmentally vulnerable region. To perform the Mann–Kendall trend test using the default significance level ($\alpha = 0.05$), and to visualize the temporal changes of the analyzed variables, as shown in Fig. 3.

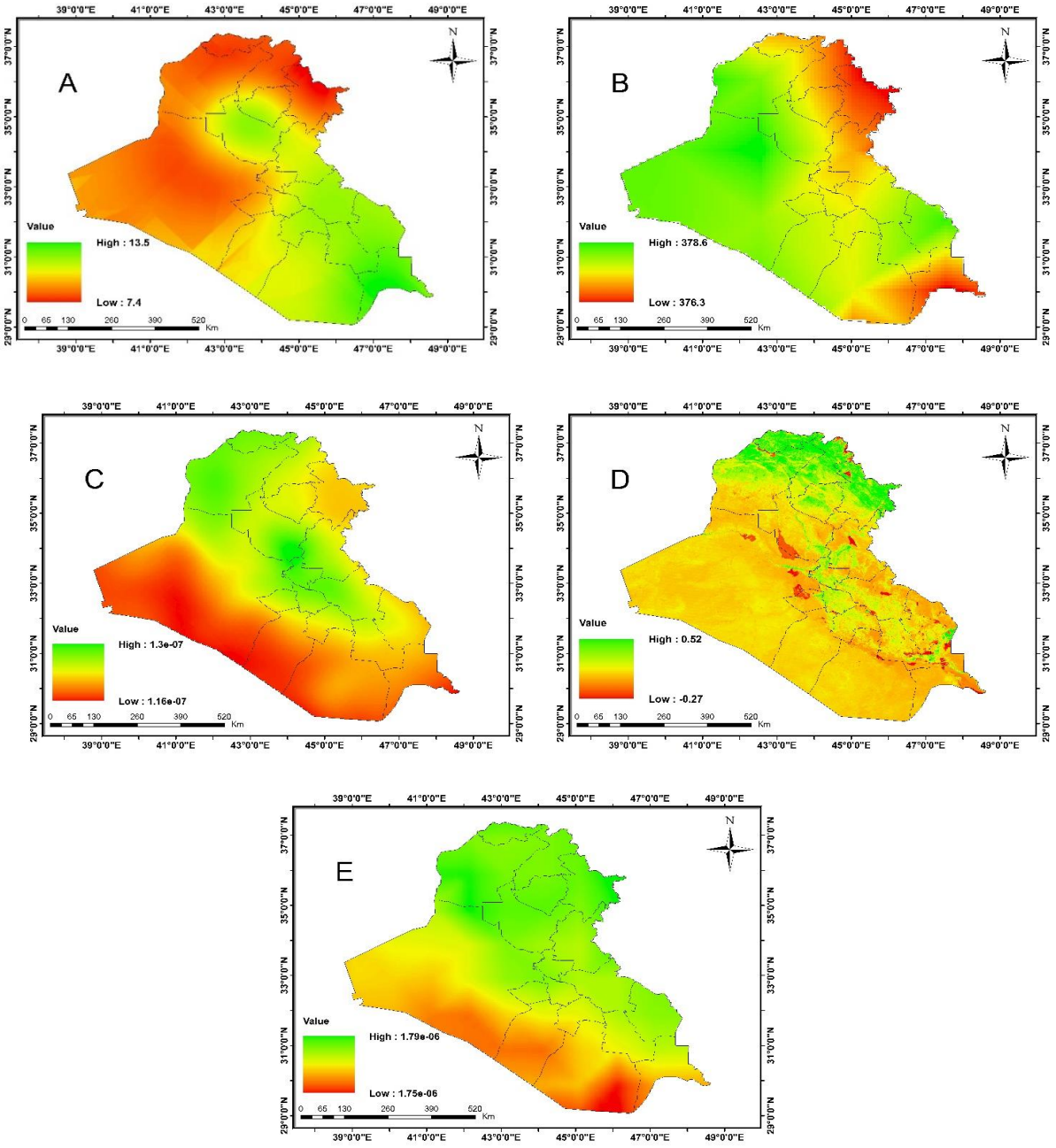

Figure 2: Examples of the datasets employed in this study: (A) air temperature (°C), (B) atmospheric CO_2 concentration (CO_2, ppm), (C) CO concentration (CO, mol mol^{-1}), (D) SAVI and (E) CH_4 concentration (CH_4, mol mol^{-1}).

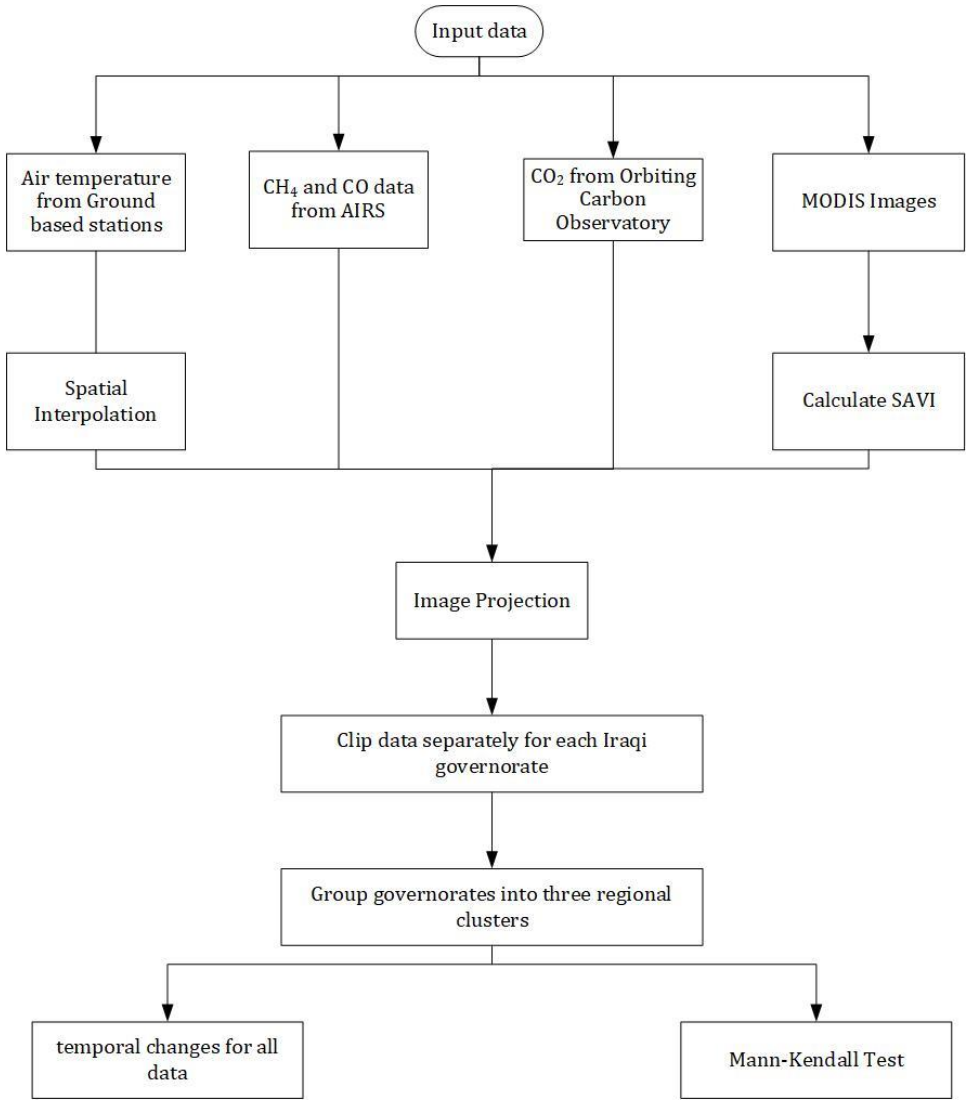

Figure (3): Block Diagram of the methodology work in this study

3.2.1 Mann-Kendall Test

The Mann–Kendall (MK) test is a widely adopted non-parametric statistical method used to detect monotonic (consistently increasing or decreasing) trends in time series data, particularly in environmental and climate-related studies [16, 17]. Being non-parametric, the MK test does not require the data to follow a normal distribution, which makes it robust to missing values, outliers, and non-normal data distributions. Given a time series dataset of size n, represented as $\{x_1, x_2, ..., x_n\}$ [16].

The MK test evaluates the sign of all pairwise differences between data points at different time steps. Specifically, for every pair where $j > i$, the difference $x_j - x_i$ is evaluated using the sign function. The Mann–Kendall statistic (S) is calculated by Eq. (1)[17]:

$$S = \sum_{i=1}^{n-1} \sum_{j=i+1}^{n} \mathrm{sgn}(x_j - x_i) \qquad (1)$$

where n represents the number of data points in the time series, x_i and x_j represent data values at times i and j, respectively.

sgn(θ) represents the sign function, defined as Eq. (2)[18]:

$$sgn(\theta) = \begin{cases} +1, & if\ \theta > 0 \\ 0\,, & if\ \theta = 0 \\ -1, & if\ \theta < 0 \end{cases} \quad (\mathbf{2})$$

Under the null hypothesis H_0 (no Temporal change), the expected value of S is zero. For sufficiently large samples (usually n>10) where n represents the sample size, the distribution of S approaches normality with variance Eq. (3) [16]:

$$\mathrm{Var(S)} = \frac{\mathrm{n(n-1)(2n+5)} - \sum_{t=1}^{m} \mathrm{t_i(t_i-1)(2t_i+5)}}{18} \quad (\mathbf{3})$$

where m represents the number of tied groups, and t_i is the size of the i^{th} tied group. The standardized test statistic Z is then calculated by Eq. (4) [16]:

$$\mathrm{Z} = \begin{cases} \dfrac{\mathrm{S-1}}{\sqrt{\mathrm{Var(S)}}}, & \mathrm{S} > 0 \\ 0\,, & \mathrm{S} = 0 \\ \dfrac{\mathrm{S+1}}{\sqrt{\mathrm{Var(S)}}}, & \mathrm{S} < 0 \end{cases} \quad (\mathbf{4})$$

The significance of the Temporal change is assessed by comparing Z to the standard normal distribution for a chosen significance level α (commonly 0.05). To quantify the rate of change (slope) in the data, the Theil-Sen estimator is used alongside the MK test. It calculates the median slope of all pairs by using Eq. (5) [17]:

$$\mathrm{Q} = \mathrm{median}\left(\frac{\mathrm{x_j - x_i}}{\mathrm{j-i}}\right), \text{for all } \mathrm{i} < \mathrm{j} \quad (\mathbf{5})$$

where Q represents the estimated slope o, x_i,x_j represent the values at time steps j and i, respectively, j−i represents the time difference between observations.

3.2.2 Soil Adjusted Vegetation Index (SAVI)

The SAVI is a spectral vegetation index designed to minimize the influence of soil brightness in areas where vegetation cover is sparse. It was introduced by Huete as a modification of the Normalized Difference Vegetation Index (NDVI) to account for the background soil reflectance [18], which often distorts vegetation signals, especially in arid and semi-arid environments. SAVI is calculated using Eq. (6) [19]:

$$\mathrm{SAVI} = \frac{(\mathrm{NIR - Red})}{(\mathrm{NIR + Red + L})} \times (\mathrm{L+1}) \quad (\mathbf{6})$$

Where NIR represents reflectance in the near-infrared band, Red = reflectance in the red band, and L represents the soil brightness correction factor; typically, L = 0.5 for intermediate vegetation densities.

3.2.3 Spatial Interpolation

Spatial interpolation is a geostatistical method used to estimate the values of variables at unsampled locations based on known values from sampled points in space. It assumes spatial autocorrelation, meaning nearby points are more likely to have similar values [20]. There are two main types: deterministic methods (Inverse Distance Weighting and spline), which rely on mathematical formulas, and geostatistical methods (Kriging), which consider both the distance and the spatial structure of the data. These methods are widely used in climatology, hydrology, and environmental sciences to generate continuous surfaces from discrete data. Proper selection of the interpolation technique depends on the nature of the dataset and the spatial variability [21]. In this paper, the Kriging method was specifically employed to generate the temperature maps.

4. Results and Discussion

The analysis of selected climatic and environmental variables is presented as follows:

4.1 Air Temperature

The analysis indicates weak to moderate positive temporal trends in monthly mean air temperature across most Iraqi provinces. The Mann–Kendall Z-values generally range between 0.87 and 3.15, with more pronounced warming trends observed in several middle and southern provinces, particularly Baghdad, Muthanna, and Najaf (Tables 2–4).

Although positive Z-values dominate the results, many monthly trends remain statistically non-significant ($|Z| \leq 1.96$), especially during February and March. In contrast, statistically significant warming signals are evident in selected months, such as January and May, reflecting the influence of seasonal variability and long-term climatic forcing.

The Avg values reported in the tables were not calculated as a simple arithmetic mean of the monthly Mann–Kendall statistics (Z and Q) displayed for January to May. Instead, the averaging procedure was performed at the data level prior to trend analysis. Specifically, for each year within the study period (2001–2024), monthly raster-based mean values (January–May) were first spatially averaged for each province. These monthly means were then aggregated to produce a single annual mean value per year. Subsequently, the Mann–Kendall test and Sen's slope estimator were applied to the resulting annual mean time series to derive the Avg Z and Q statistics. Therefore, the Avg row represents the overall temporal trend of the interannual mean conditions for the January–May period, rather than the arithmetic average of the individual monthly Z or Q values shown in the tables.

Table 2: Monthly and annual-average Mann–Kendall (Z) and Sen's slope (Q) statistics for air temperature trends in northern Iraqi provinces during the period 2003–2024.

Month	Duhok		Erbil		Nineveh		Sulaymaniyah	
	Q	Z	Q	Z	Q	Z	Q	Z
Jan	0.02	0.37	0.05	0.77	0.07	1.41	0.05	1.86
Feb	0.08	1.71	0.09	2.21	0.08	1.71	0.09	2.31
Mar	-0.08	-0.97	-0.06	-0.67	-0.05	-0.77	-0.04	-0.77
Apr	0.15	1.61	0.10	1.81	0.10	1.71	0.04	0.57
May	-0.01	-0.21	-0.06	-1.11	0.00	0.11	-0.01	-0.16
Avg	0.04	1.12	0.01	0.87	0.05	1.76	0.03	1.12

Table 3: Monthly and annual-average Mann–Kendall (Z) and Sen's slope (Q) statistics for air temperature trends in middle Iraqi provinces during the period 2003–2024.

Month	Baghdad		Babil		Anbar		Salah ad Din	
	Q	Z	Q	Z	Q	Z	Q	Z
Jan	0.11	2.85	0.07	1.86	0.07	1.71	0.08	1.27
Feb	0.06	1.17	0.02	0.42	0.06	1.36	0.09	1.36
Mar	0.03	0.72	-0.03	-0.67	-0.03	-0.42	0.02	0.22
Apr	0.05	1.02	0.04	0.87	0.08	1.71	0.10	1.76
May	0.02	0.58	0.02	0.42	0.04	0.90	0.02	0.58
Avg	0.07	2.80	0.04	1.41	0.05	2.11	0.09	2.55

Table 4: Monthly and annual-average Mann–Kendall (Z) and Sen's slope (Q) statistics for air temperature trends in southern Iraqi provinces during the period 2003–2024.

Month	Basra		Maysan		Muthanna		Najaf	
	Q	Z	Q	Z	Q	Z	Q	Z
Jan	0.09	2.60	0.07	2.51	0.10	1.91	0.11	2.51
Feb	0.04	0.87	0.06	1.22	0.05	1.07	0.07	1.81
Mar	-0.01	-0.37	0.01	0.22	0.04	0.77	0.03	0.72
Apr	0.03	0.72	0.03	0.82	0.04	1.56	0.06	1.96
May	0.02	0.48	-0.05	-1.32	0.08	2.01	0.09	2.11
Avg	0.05	2.11	0.04	1.46	0.08	2.95	0.08	3.15

The air temperature (°C) for Iraqi regions during the period 2003 to 2024 is illustrated in Fig. (4-6). The time series exhibits a pronounced seasonal cycle, characterized by regular and recurrent oscillations corresponding to annual temperature variability. These oscillations reflect the alternation between higher temperatures during warm seasons and lower temperatures during cold seasons, indicating a strong seasonal signal throughout the entire observation period.

In addition to the seasonal variability, the dashed trend line indicates a slight but consistent long-term increase in mean air temperature over time. Although short-term fluctuations are evident, the overall trend suggests gradual warming across the study period. This upward tendency becomes more apparent when considering the cumulative behavior of the time series rather than individual years, emphasizing the presence of long-term climatic change superimposed on seasonal patterns. Moreover, the amplitude of seasonal temperature variations remains relatively stable over time, suggesting that while average temperatures are increasing, the contrast between warm and cold seasons has not undergone substantial alteration. Occasional extreme values are observed; however, these deviations do not significantly disrupt the general seasonal structure or the long-term trend. Overall, the temporal pattern of air temperature is dominated by strong seasonal variability combined with a gradual increasing trend, highlighting the importance of distinguishing between short-term seasonal dynamics and long-term climatic signals when analyzing temperature time series.

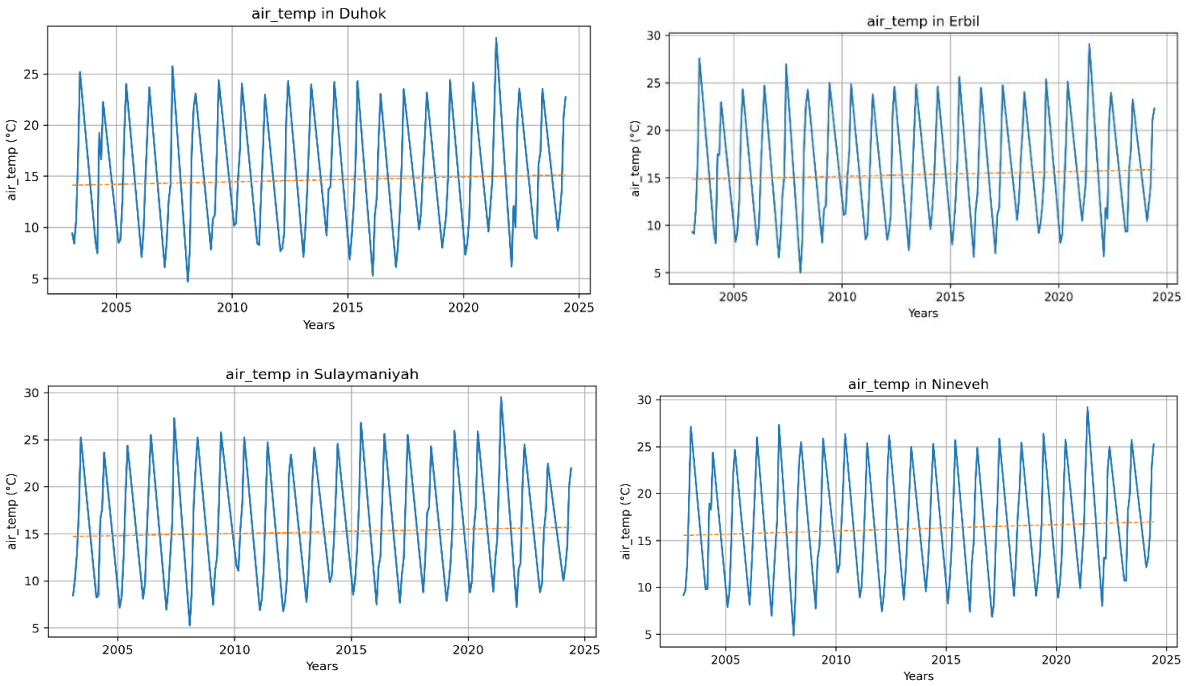

Figure 4: Air temperature in the northern Iraqi regions during the period 2003-2024.

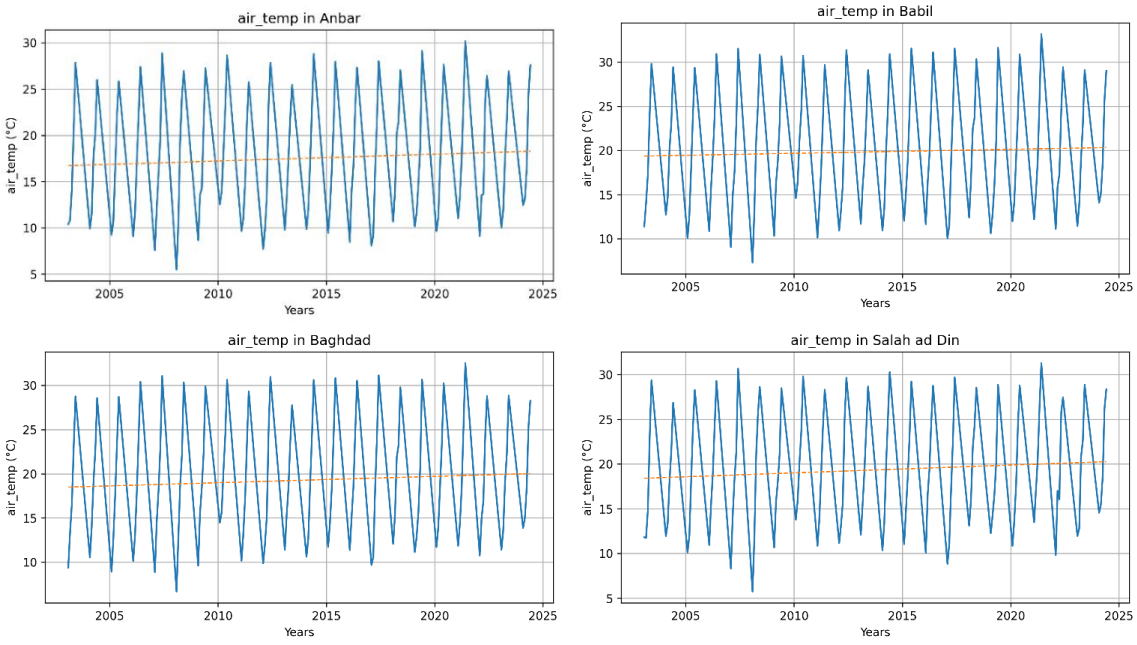

Figure 5: Air temperature in the middle Iraqi regions during the period 2003-2024.

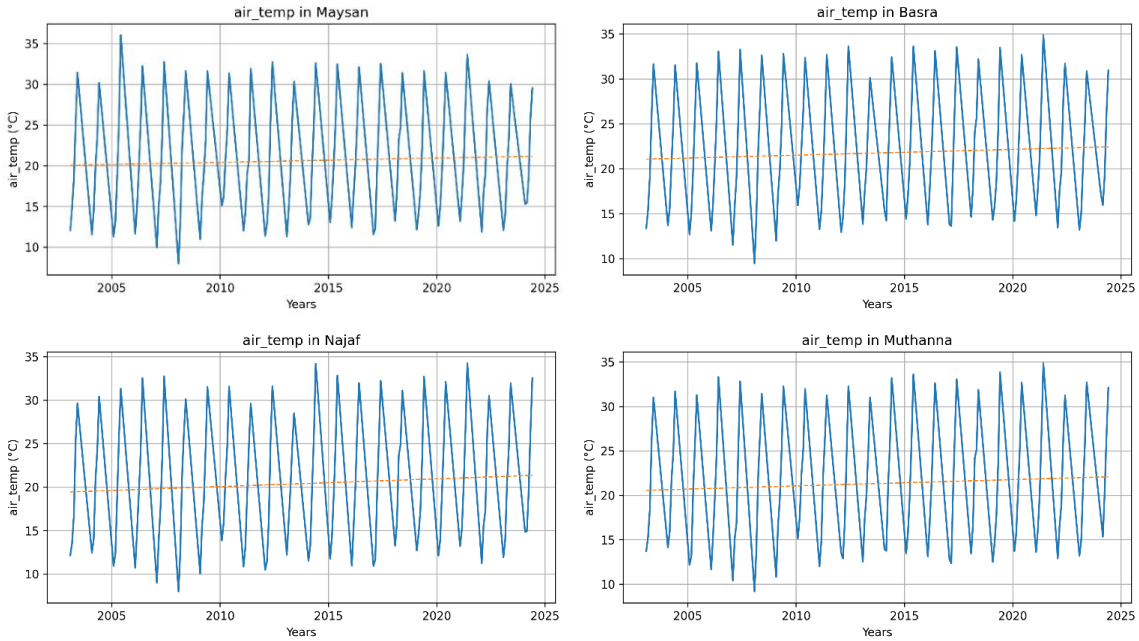

Figure 6: Air temperature in the Southern Iraqi regions during the period 2003-2024.

4.2. Methane (CH_4)

A consistently strong and statistically significant increase in CH_4 mol mol^{-1} concentration was observed across all Iraqi provinces and throughout the year. All Northern provinces exhibit strong, consistent positive temporal changes in CH4 concentrations, with Sen's slope values ranging from 2.6×10^{-9} to 3.7×10^{-9} (mol $mol^{-1}year^{-1}$). The Mann-Kendall test is highly significant, ranging between 5.64 and 6.20, well above the 99% confidence threshold. March notably shows the greatest and most consistent upward temporal changes across all provinces. Among these, Nineveh demonstrates the most pronounced increase, followed by Duhok, while Erbil and Sulaymaniyah maintain slightly lower but still robust upward Temporal changes as demonstrated in the Table 5. Middle provinces also display statistically significant upward Temporal changes with Q-values between 2.7×10^{-9} and 3.8×10^{-9} (mol $mol^{-1}year^{-1}$) and Z-values ranging from 5.75 to 6.26. February and March mark peak periods of temporal change strength. Anbar records the steepest rate of increase, whereas Baghdad and Babylon show moderate but steady upward temporal change, see Table 6. Southern provinces reflect similarly great positive Temporal changes, with Q-values from approximately 2.2×10^{-9} up to 4.3×10^{-9} (mol $mol^{-1}year^{-1}$), and Z-values spanning 5.70 to 6.32. March and April represent the months with the most significant upward momentum, especially in Muthanna. While Basra, despite relatively lower Q-values, maintains statistically significant Temporal changes as shown in Table 7.

Table 5: Monthly and annual-average Mann–Kendall (Z) and Sen's slope (Q) statistics for CH_4 trends in northern Iraqi regions during the period 2003 -2024.

Month	Duhok		Erbil		Nineveh		Sulaymaniyah	
	Q	Z	Q	Z	Q	Z	Q	Z
Jan	3.1E-09	5.75	2.6E-09	5.98	3.5E-09	6.03	2.8E-09	6.03
Feb	3.0E-09	6.09	2.6E-09	5.70	3.2E-09	5.81	2.7E-09	6.03
Mar	3.4E-09	6.03	2.9E-09	6.03	3.7E-09	6.03	3.0E-09	5.98
Apr	3.1E-09	6.03	2.7E-09	5.92	3.4E-09	6.20	2.9E-09	5.92
May	3.2E-09	5.98	2.7E-09	5.98	3.5E-09	5.92	2.9E-09	6.03
Avg	3.1E-09	6.15	2.7E-09	6.15	3.6E-09	6.09	2.9E-09	6.20

Table 6: Monthly and annual-average Mann–Kendall (Z) and Sen's slope (Q) statistics for CH_4 trends in the middle Iraqi regions during the period 2003 -2024.

Month	Baghdad		Babil		Anbar		Salah ad Din	
	Q	Z	Q	Z	Q	Z	Q	Z
Jan	2.9E-09	6.03	2.9E-09	6.09	3.4E-09	5.98	2.9E-09	5.98
Feb	2.7E-09	6.20	2.9E-09	6.20	3.4E-09	6.03	2.8E-09	6.15
Mar	2.9E-09	6.15	3.1E-09	6.20	3.8E-09	6.03	3.1E-09	6.15
Apr	2.8E-09	6.03	2.8E-09	5.98	3.8E-09	5.92	2.8E-09	6.20
May	2.8E-09	5.92	2.9E-09	5.75	3.7E-09	5.87	2.8E-09	5.92
Avg	2.8E-09	6.09	2.9E-09	6.20	3.6E-09	6.09	2.9E-09	6.15

Table 7: Monthly and annual-average Mann–Kendall (Z) and Sen's slope (Q) statistics for CH_4 trends in southern Iraqi regions during the period 2003 -2024.

Month	Basra		Maysan		Muthanna		Najaf	
	Q	Z	Q	Z	Q	Z	Q	Z
Jan	2.2E-09	5.98	3.6E-09	6.20	3.6E-09	5.70	3.4E-09	6.03
Feb	2.4E-09	5.81	3.5E-09	5.98	3.9E-09	5.92	3.6E-09	6.03
Mar	2.4E-09	6.15	3.6E-09	6.26	4.2E-09	5.98	4.1E-09	5.98
Apr	2.3E-09	6.03	3.4E-09	6.09	4.2E-09	6.03	3.9E-09	5.92
May	2.3E-09	6.09	3.5E-09	6.03	4.3E-09	5.87	3.9E-09	5.81
Avg	2.3E-09	6.20	3.5E-09	6.26	4.0E-09	5.98	3.7E-09	5.98

CH_4 levels exhibit a steady rise across Iraqi provinces, mirroring global Temporal changes as shown in Figs. 7-9. All figures show a clear and persistent upward trend over the studied time period, indicating a gradual and sustained increase in their values with time. Although short-term fluctuations are evident throughout the series, these variations remain largely confined around the long-term trend line and do not alter the overall increasing pattern. The temporal record reveals recurrent oscillations characterized by alternating periods of relative increase and decrease. However, both the lower and upper bounds of these fluctuations rise progressively over the years, suggesting that the variability occurs around an increasingly higher baseline rather than representing random or isolated anomalies. This behavior reflects a systematic long-term change in the underlying process governing the variable.

CH_4 concentrations showed almost linear increasing during the study, suggesting that emissions are not just increasing, but doing so at a persistent rate. This trend is a clear byproduct of local industrial and human activity. Looking at the northern governorates (such as Nineveh and Dohuk), the rise is likely driven by agriculture, livestock, and waste decay, coupled with nearby energy facilities. Central regions, however, face a different set of drivers: rapid urbanization, trash management issues, and transport emissions. The most significant spikes appear in the south, where heavy oil extraction and widespread gas flaring remain the primary culprits.

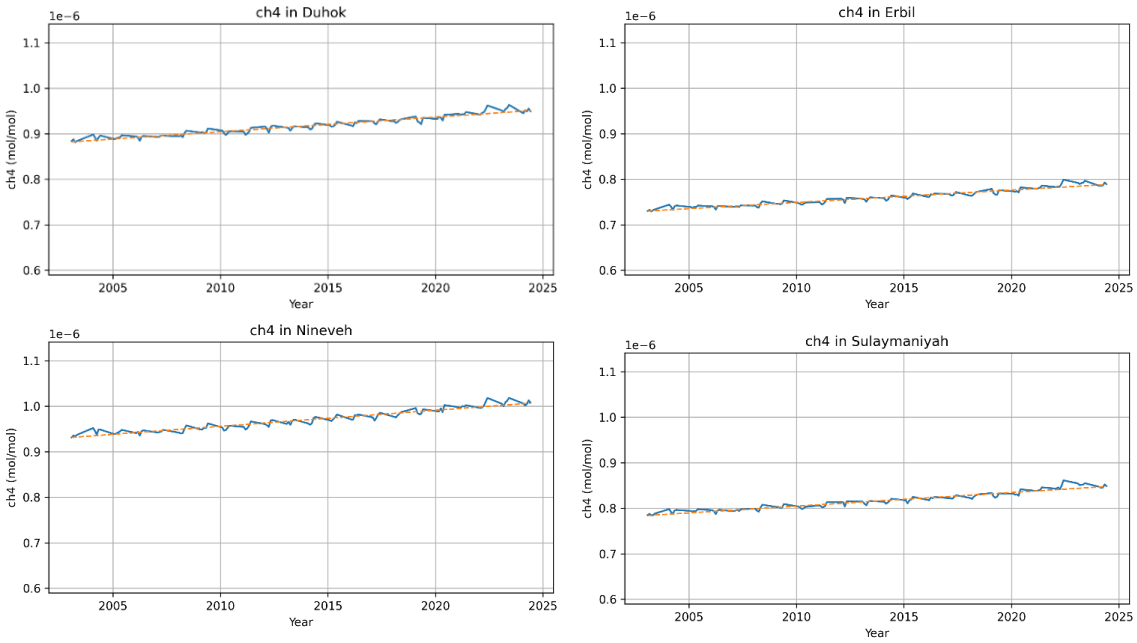

Figure 7: CH_4 in the northern Iraqi regions during the period 2003-2024.

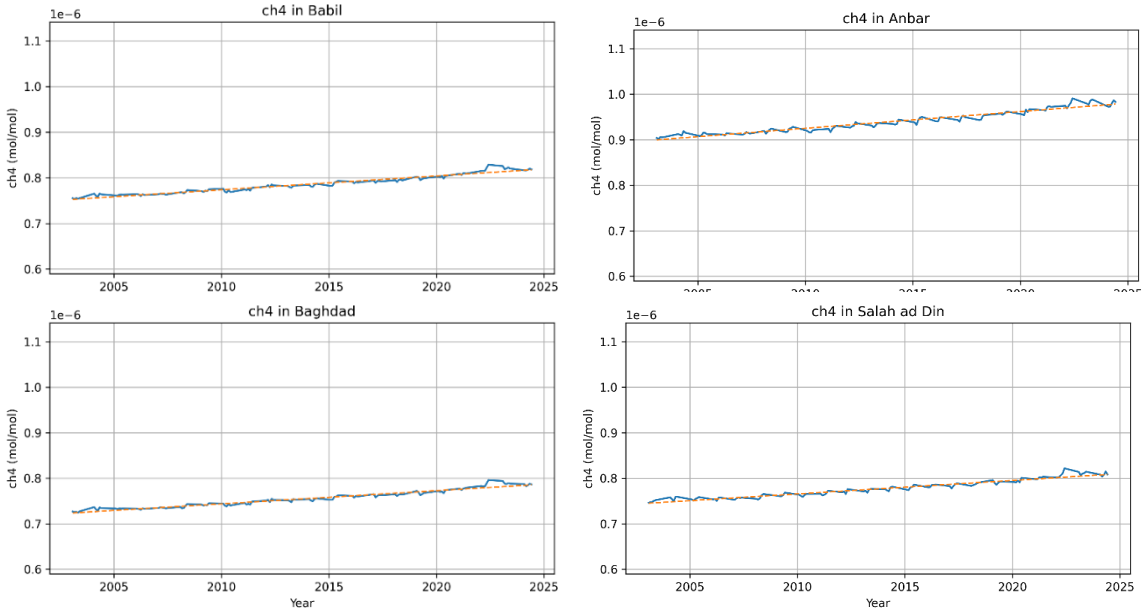

Figure 8: CH_4 in the middle Iraqi regions during the period 2003-2024.

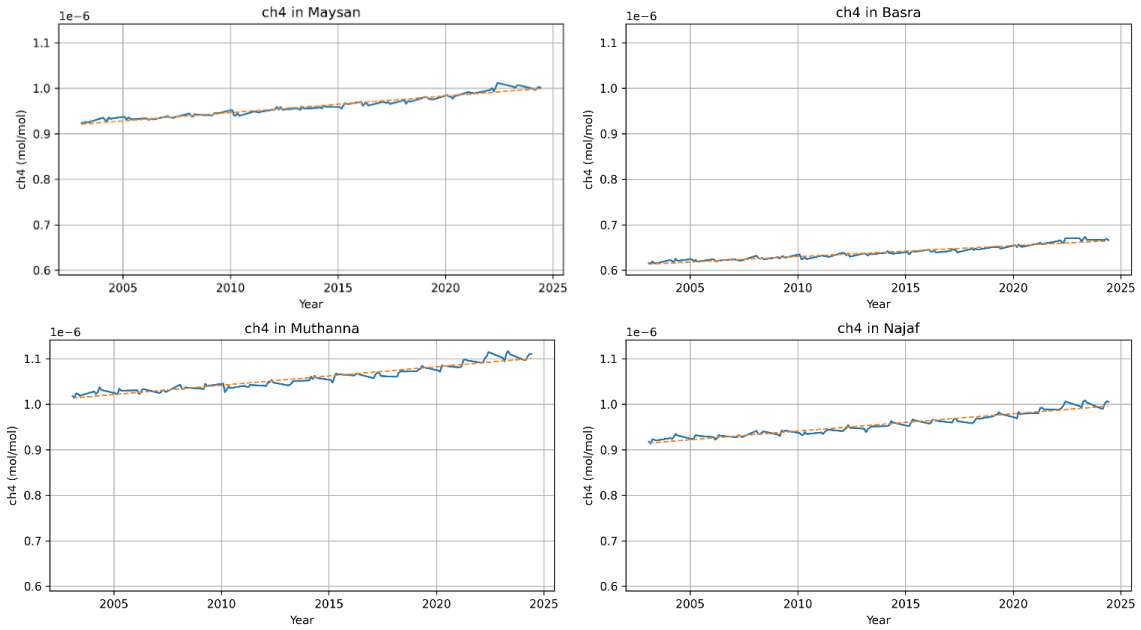

Figure 9: CH_4 in the Southern Iraqi regions during the period 2003-2024.

4.3 Carbon Monoxide (CO)

The Mann-Kendall analysis of CO concentrations across northern, middle, and southern Iraqi provinces from January to May indicates a consistent and statistically significant decline. Sen's slope (Q) values are uniformly negative, ranging from -7.2×10^{-10} to -2.1×10^{-9}, while corresponding Z-values span -4.85 to -5.98, all exceeding the 99% confidence threshold (Tables 8–10), confirming the robustness of this downward trend .Seasonally, the rate of decline varies across regions. In the north, the steepest decreases occur in March–May, particularly in Nineveh and Sulaymaniyah. Middle provinces, such as Anbar and Salah ad Din, show peak reductions in February and March, whereas southern provinces, notably Muthanna and Najaf, reach maximum decline mainly in March and April. Basra exhibits smaller slopes but maintains a consistent decrease throughout the period. Spatially, the greatest reductions are observed in northern provinces, followed by middle regions, with southern provinces showing slightly smaller yet significant declines.

Table 8: Monthly and annual-average Mann–Kendall (Z) and Sen's slope (Q) statistics for CO trends in northern Iraqi regions during the period 2003 -2024.

Month	Duhok		Erbil		Nineveh		Sulaymaniyah	
	Q	Z	Q	Z	Q	Z	Q	Z
Jan	-1.5E-09	-4.96	-1.1E-09	-5.08	-1.7E-09	-5.02	-1.2E-09	-5.24
Feb	-2.0E-09	-4.85	-1.5E-09	-5.02	-2.1E-09	-5.02	-1.5E-09	-5.30
Mar	-1.6E-09	-5.19	-1.5E-09	-4.91	-1.9E-09	-5.30	-1.6E-09	-5.19
Apr	-1.9E-09	-5.02	-1.6E-09	-5.08	-2.0E-09	-5.08	-1.5E-09	-5.08
May	-1.4E-09	-5.19	-1.3E-09	-5.41	-1.6E-09	-5.41	-1.4E-09	-5.02
Avg	-1.7E-09	-5.47	-1.4E-09	-5.64	-1.8E-09	-5.87	-1.4E-09	-5.87

Table :9 Monthly and annual-average Mann–Kendall (Z) and Sen's slope (Q) statistics for CO trends in middle Iraqi regions during the period 2003 -2024.

Month	Baghdad		Babil		Anbar		Salah ad Din	
	Q	Z	Q	Z	Q	Z	Q	Z
Jan	-1.3E-09	-5.36	-1.3E-09	-5.41	-1.7E-09	-5.30	-1.3E-09	-5.64
Feb	-1.4E-09	-5.70	-1.5E-09	-5.41	-1.8E-09	-5.47	-1.5E-09	-5.64
Mar	-1.5E-09	-5.47	-1.6E-09	-5.53	-1.9E-09	-5.30	-1.6E-09	-5.41
Apr	-1.5E-09	-5.36	-1.5E-09	-5.30	-1.8E-09	-5.19	-1.5E-09	-5.13
May	-1.3E-09	-5.24	-1.3E-09	-5.19	-1.3E-09	-5.19	-1.4E-09	-5.19
Avg	-1.4E-09	-5.87	-1.4E-09	-5.87	-1.8E-09	-5.92	-1.5E-09	-5.87

Table 10: Monthly and annual-average Mann–Kendall (Z) and Sen's slope (Q) statistics for CO trends in southern Iraqi regions during the period 2003 -2024.

Month	Basra		Dhi Qar		Maysan		Muthanna	
	Q	Z	Q	Z	Q	Z	Q	Z
Jan	-9.1E-10	-5.81	-1.5E-09	-5.64	-1.5E-09	-5.58	-1.9E-09	-5.41
Feb	-1.0E-09	-5.47	-1.7E-09	-5.53	-1.7E-09	-5.58	-2.1E-09	-5.36
Mar	-1.1E-09	-5.47	-1.7E-09	-5.70	-1.7E-09	-5.70	-2.2E-09	-5.41
Apr	-1.0E-09	-5.36	-1.7E-09	-5.24	-1.8E-09	-5.24	-2.1E-09	-5.41
May	-7.2E-10	-5.19	-1.3E-09	-5.47	-1.4E-09	-5.24	-1.6E-09	-5.47
Avg	-9.5E-10	-5.92	-1.6E-09	-5.81	-1.6E-09	-5.75	-1.9E-09	-5.98

The CO concentration shows a fluctuating yet overall declining temporal change from 2003 to 2024, see Figs. 10-12. As shown in the figures, the examined variable demonstrates a clear long-term decreasing trend over the analyzed time period, indicating a gradual and consistent decline in its values with time. Despite the presence of pronounced short-term fluctuations, the overall trajectory remains distinctly downward, as confirmed by the negative slope of the fitted trend line. The time series is characterized by recurrent oscillations around the long-term trend, reflecting notable short-term variability. However, both the peak and trough values exhibit a progressive decline through time, suggesting that these fluctuations occur around a steadily lowering baseline rather than representing random variability. This pattern points to a systematic long-term reduction in the magnitude of the variable.

Moreover, the decline appears approximately linear across much of the study period, implying a relatively stable rate of decrease and a sustained influence of the controlling factors over time. In general, the temporal behavior of this variable can be described as a dominant long-term downward trend accompanied by moderate to strong short-term variability, a pattern commonly observed in environmental time series subject to gradual regulatory, atmospheric, or climatic influences.

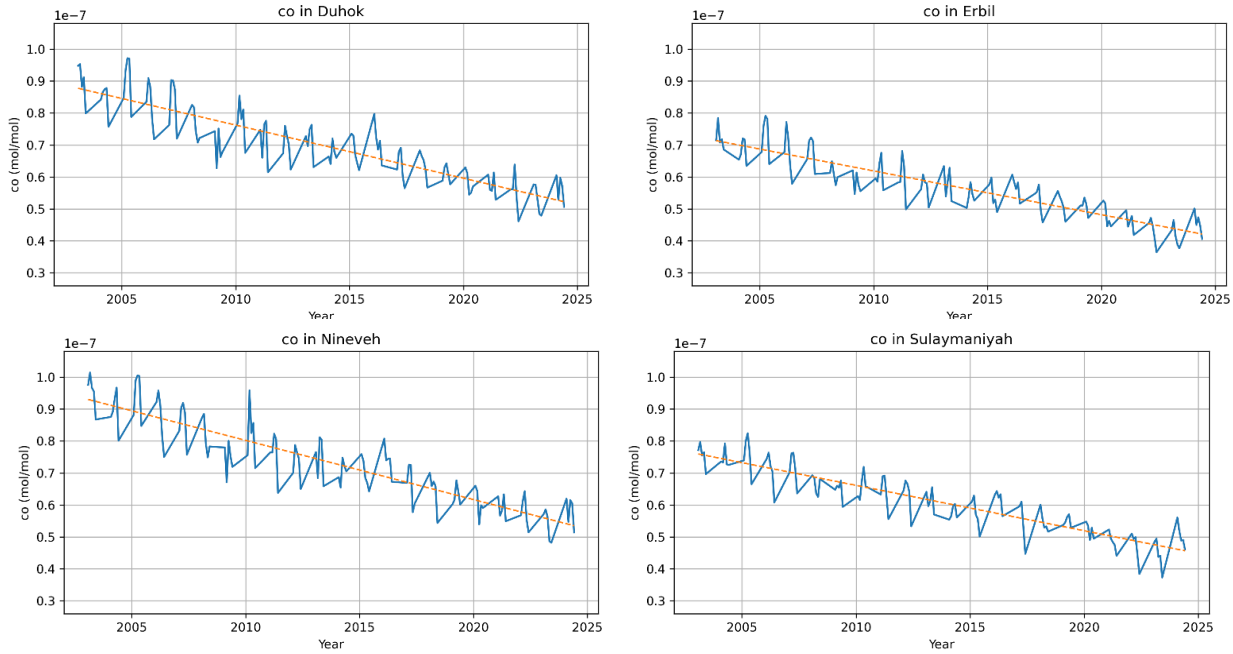

Figure 10: CO in the northern Iraqi regions during the period 2003-2024.

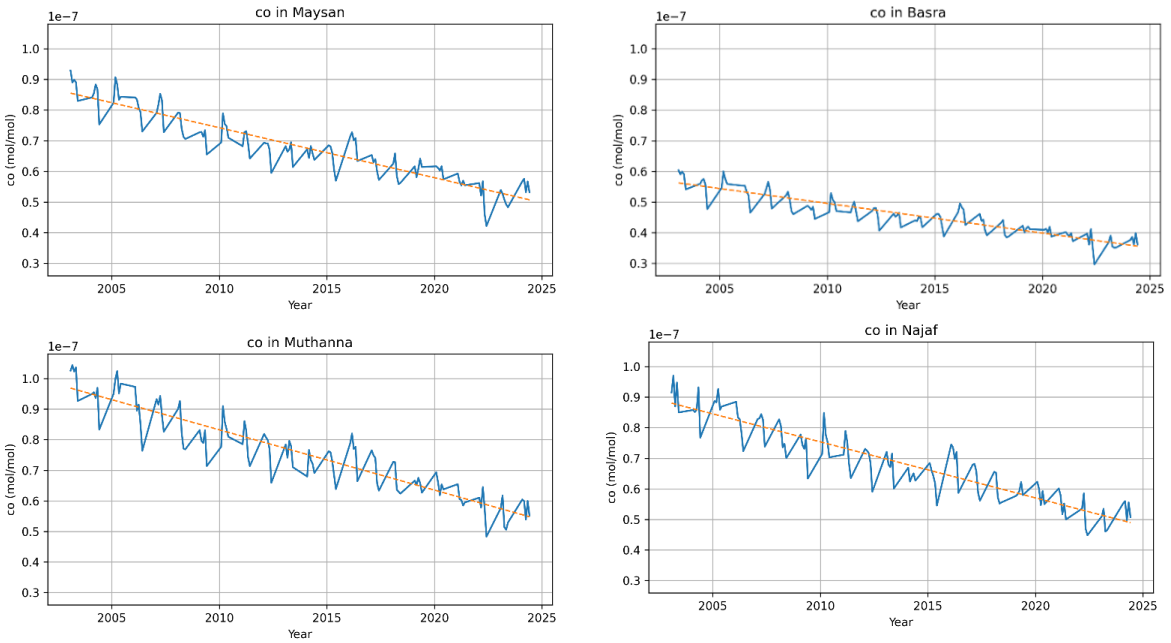

Figure 11: CO in the middle Iraqi regions during the period 2003-2024.

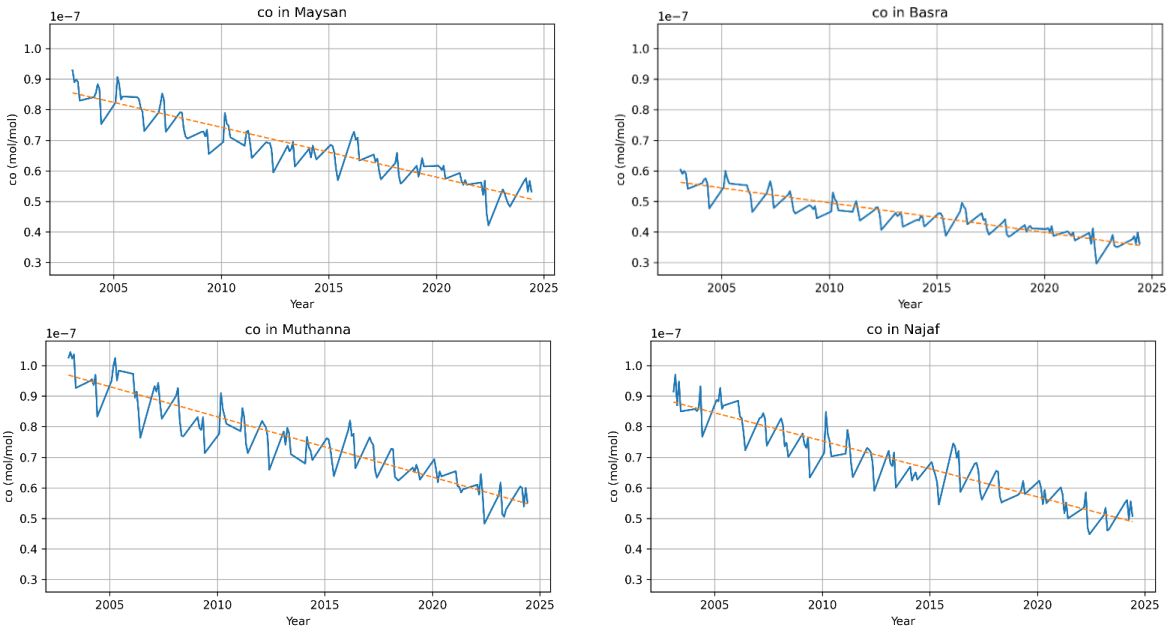

Figure 12: CO in the southern Iraqi regions during the period 2003-2024.

4.4. Carbon Dioxide (CO_2)

CO_2 concentrations exhibited an extremely strong, consistent, and statistically significant upward temporal change across all provinces and throughout the year. Z-values were remarkably uniform, averaging around 6.4 to 6.49 in all months and regions, indicating a pervasive and accelerating increase in CO_2 levels, as displayed in Tables (11–13). The Sen's slope (Q) values, representing the annual rate of increase, range approximately between 2.23 and 2.35 ppm/year, quantitatively defining the yearly rise in CO_2 concentration .This homogeneity in both Z and Q-values underscores the global nature of CO_2 accumulation in the atmosphere, driven by sustained and cumulative emissions. The consistent rise across Iraq, including northern regions, reflects broader climate change trajectories, confirming that local temporal changes align with the long-term global pattern of increasing greenhouse gas concentrations.

Table 11: Monthly and annual-average Mann–Kendall (Z) and Sen's slope (Q) statistics for *CO_2* trends in northern Iraqi regions during the period 2003 -2024.

Month	Duhok		Erbil		Nineveh		Sulaymaniyah	
	Q	Z	Q	Z	Q	Z	Q	Z
Jan	2.30	6.37	2.29	6.43	2.30	6.43	2.29	6.43
Feb	2.33	6.49	2.29	6.43	2.29	6.49	2.29	6.49
Mar	2.25	6.43	2.23	6.43	2.23	6.49	2.23	6.43
Apr	2.29	6.49	2.27	6.49	2.23	6.49	2.28	6.43
May	2.24	6.43	2.28	6.49	2.26	6.49	2.31	6.49
Avg	2.29	6.49	2.28	6.49	2.26	6.49	2.28	6.49

Table 12: Monthly and annual-average Mann–Kendall (Z) and Sen's slope (Q) statistics for CO_2 trends in middle Iraqi regions during the period 2003 -2024.

Month	Baghdad		Babil		Anbar		Salah ad Din	
	Q	Z	Q	Z	Q	Z	Q	Z
Jan	2.30	6.49	2.30	6.49	2.32	6.49	2.29	6.49
Feb	2.25	6.43	2.23	6.43	2.29	6.49	2.26	6.43
Mar	2.24	6.37	2.28	6.43	2.21	6.43	2.23	6.43
Apr	2.26	6.37	2.27	6.43	2.21	6.43	2.27	6.32
May	2.29	6.49	2.31	6.49	2.22	6.49	2.27	6.49
Avg	2.27	6.43	2.28	6.49	2.25	6.49	2.26	6.49

Table 13: Monthly and annual-average Mann–Kendall (Z) and Sen's slope (Q) statistics for CO_2 trends in southern Iraqi regions during the period 2003 -2024.

Month	Basra		Maysan		Muthanna		Najaf	
	Q	Z	Q	Z	Q	Z	Q	Z
Jan	2.31	6.43	2.35	6.49	2.27	6.49	2.29	6.49
Feb	2.29	6.43	2.28	6.43	2.24	6.49	2.24	6.49
Mar	2.28	6.49	2.27	6.43	2.24	6.37	2.23	6.43
Apr	2.33	6.49	2.31	6.49	2.30	6.49	2.23	6.43
May	2.35	6.43	2.34	6.43	2.31	5.87	2.26	6.43
Avg	2.32	6.49	2.30	6.49	2.27	5.87	2.25	6.49

The concentration of CO_2 exhibits a steady and continuous upward trend over time. The temporal variations and rate of increase are illustrated in Figs. 13–15. The analyzed variable displays a strong and persistent increasing trend over the entire study period, reflecting a continuous rise in its values with time. The temporal pattern is characterized by a remarkably consistent upward trajectory, as evidenced by the close agreement between the observed values and the fitted trend line. Short-term fluctuations are present but remain relatively small in magnitude compared to the overall increase, indicating limited interannual variability. These minor deviations around the long-term trend do not disrupt the dominant pattern of growth; instead, they suggest stable system behavior with modest temporal variability. The increase appears largely linear throughout the observation period, implying a steady rate of change and a sustained influence of the driving factors over time. Overall, the time series can be described as exhibiting a pronounced long-term upward trend with minimal short-term variability, a behavior commonly observed in atmospheric and environmental variables influenced by cumulative and persistent forcing mechanisms.

4.5. SAVI

The SAVI analysis (2003–2024) revealed substantial spatial and temporal variability in vegetation across Iraq. Northern provinces such as Erbil and Sulaymaniyah showed significant positive trends ($Z > 2.0$), particularly in March and April, while Duhok exhibited only sporadic increases. Conversely, Nineveh experienced weak or negative trends, indicating localized vegetation stress as demonstrated in the Tables (14-16). In central Iraq, Babil displayed strong improvements ($Z > 4.0$), whereas Anbar showed no meaningful change ($Z \approx -0.12$). Southern regions, particularly Basra, experienced weak or declining trends ($Z = 0.72$), highlighting potential environmental degradation, while Maysan, Muthanna, and Najaf showed modest positive changes. Overall, these findings underscore marked disparities in vegetation dynamics, with some regions improving and others stagnating or declining. The results highlight the urgency of targeted

ecological measures in areas exhibiting weak or negative trends to mitigate vegetation loss and support sustainable land management.

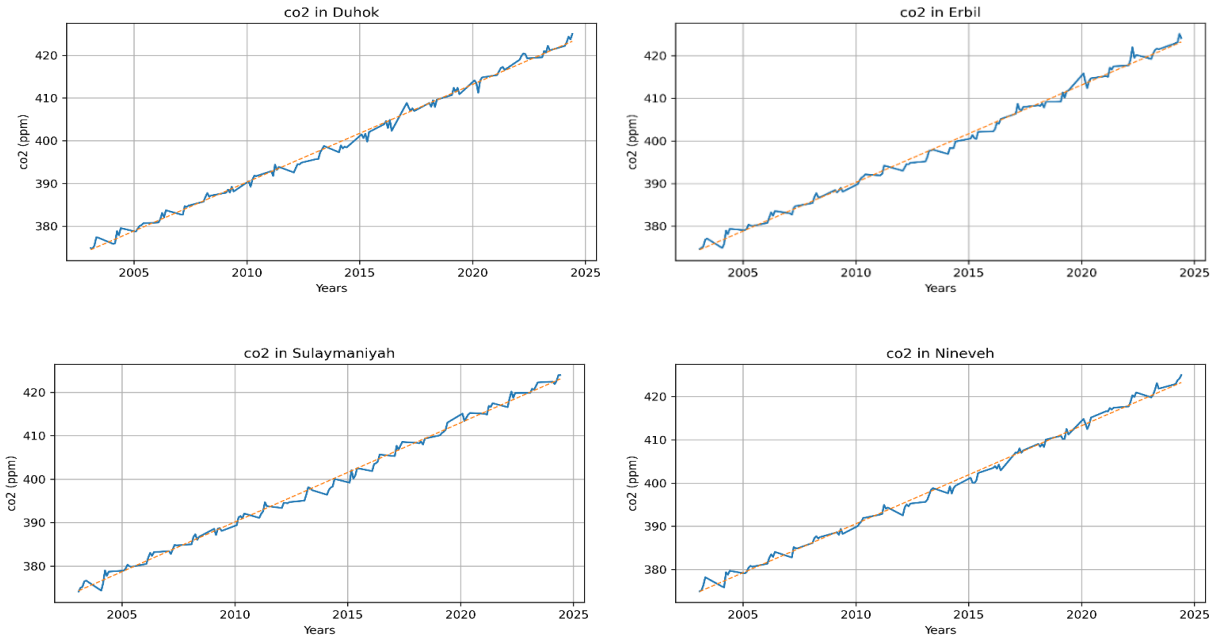

Figure 13: Carbon Dioxide in the northern Iraqi regions during the period 2003-2024.

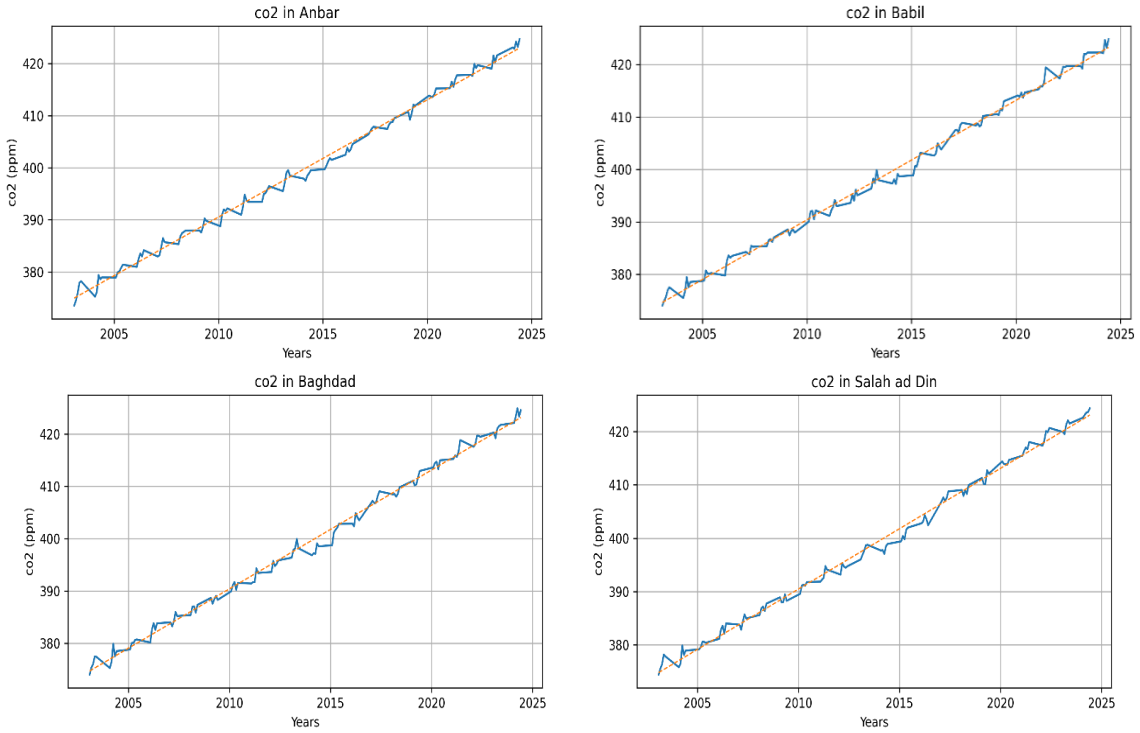

Figure 14: Carbon Dioxide in the middle Iraqi regions during the period 2003-2024.

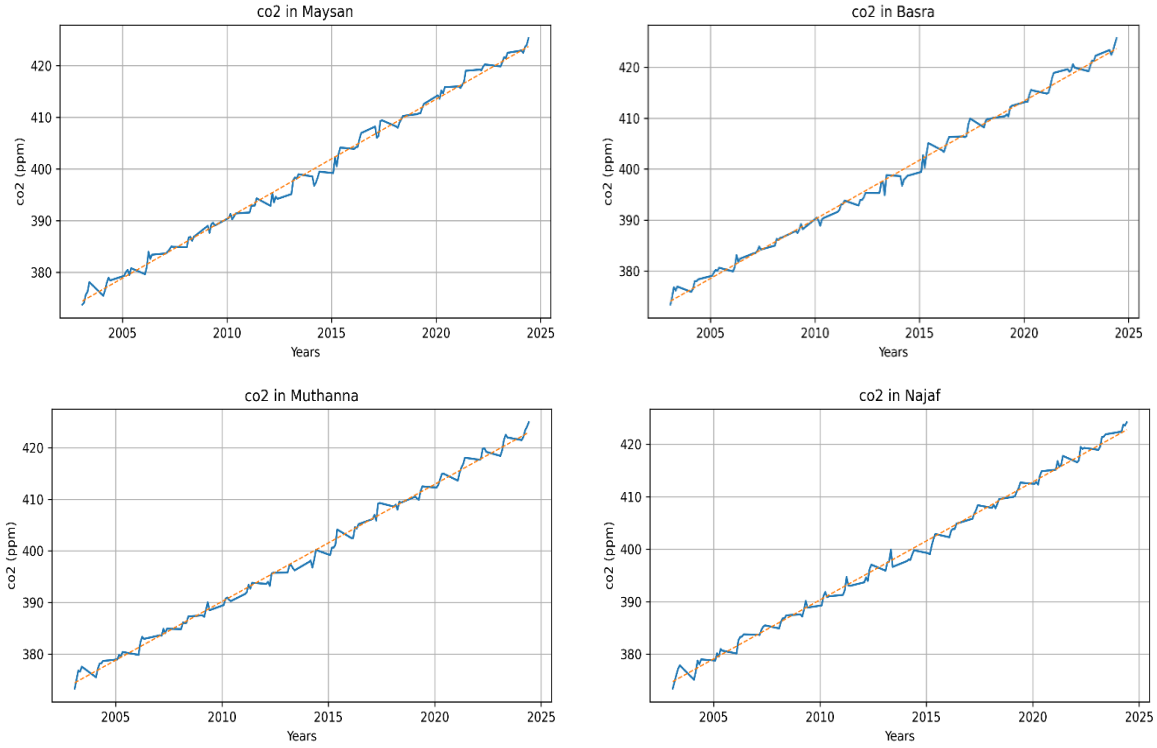

Figure 15: Carbon Dioxide in the southern Iraqi regions during the period 2003-2024.

Table 14: Monthly and annual-average Mann–Kendall (Z) and Sen's slope (Q) statistics for SAVI trends in northern Iraqi regions during the period 2003 -2024.

Month	Duhok		Erbil		Nineveh		Sulaymaniyah	
	Q	Z	Q	Z	Q	Z	Q	Z
Jan	1.3E-03	1.02	2.5E-03	2.06	7.7E-04	1.02	3.1E-03	2.36
Feb	1.7E-03	1.51	3.5E-03	2.06	1.5E-03	0.92	3.0E-03	1.81
Mar	2.6E-03	2.01	4.7E-03	2.65	1.0E-03	0.62	3.9E-03	2.65
Apr	1.5E-04	0.12	2.7E-03	1.71	-8.3E-04	-0.67	2.8E-03	2.11
May	-1.2E-04	-0.07	7.6E-04	0.97	-4.7E-04	-0.47	3.5E-04	0.42
Avg	1.5E-03	1.96	2.8E-03	2.70	9.1E-05	0.07	2.6E-03	2.75

Table 15: Monthly and annual-average Mann–Kendall (Z) and Sen's slope (Q) statistics for SAVI using the MK test for middle Iraqi regions during the period 2003 -2024.

Month	Baghdad		Babil		Anbar		Salah ad Din	
	Q	Z	Q	Z	Q	Z	Q	Z
Jan	1.2E-03	1.22	2.7E-03	3.10	-5.5E-05	-0.17	2.0E-03	2.06
Feb	9.8E-04	0.57	2.7E-03	2.31	4.8E-05	0.27	2.2E-03	1.27
Mar	1.4E-03	1.46	3.0E-03	2.90	3.4E-05	0.07	1.8E-03	1.46
Apr	1.5E-03	2.16	2.4E-03	4.04	2.3E-04	1.76	1.7E-03	2.51
May	1.4E-05	0.00	9.8E-04	2.01	1.5E-04	1.31	4.3E-04	1.41
Avg	1.1E-03	1.46	2.5E-03	3.45	-9.2E-06	-0.12	1.4E-03	1.61

Table 16: Monthly and annual-average Mann–Kendall (Z) and Sen's slope (Q) statistics for SAVI trends in the southern Iraqi regions during the period 2003 -2024.

Month	Basra		Maysan		Muthanna		Najaf	
	Q	Z	Q	Z	Q	Z	Q	Z
Jan	4.7E-04	2.21	1.5E-03	2.41	8.5E-04	2.36	6.3E-04	2.16
Feb	4.6E-04	0.92	1.3E-03	1.07	6.3E-04	1.27	6.6E-04	1.12
Mar	-1.1E-05	-0.02	1.1E-03	1.51	3.3E-04	1.07	3.8E-04	1.31
Apr	-3.1E-05	-0.22	8.7E-04	2.41	3.9E-04	2.11	5.3E-04	3.20
May	-2.6E-04	-1.36	4.2E-04	1.07	1.6E-04	1.51	2.9E-04	1.96
Avg	9.3E-05	0.72	1.1E-03	1.51	3.8E-04	1.41	4.5E-04	1.91

The SAVI index reveals a declining temporal change in many provinces, as shown in Figs. (16-18), signaling reduced vegetation health or coverage. This decline is linked to prolonged droughts, desertification, and urban encroachment on agricultural land.

The SAVI displays marked interannual fluctuations around a mean of ~0.20 from 2005–2025, with peaks above 0.30 and troughs near zero, overlaid by a subtle upward linear trend indicating gradual vegetation enhancement. This oscillatory pattern reflects pulsed responses to rainfall variability in semi-arid settings, underscoring SAVI's utility for tracking dynamic soil-vegetation interactions amid climatic forcing. Values consistently above 0.10 confirm moderate greenness resilience, punctuated by transient bare-soil phases.

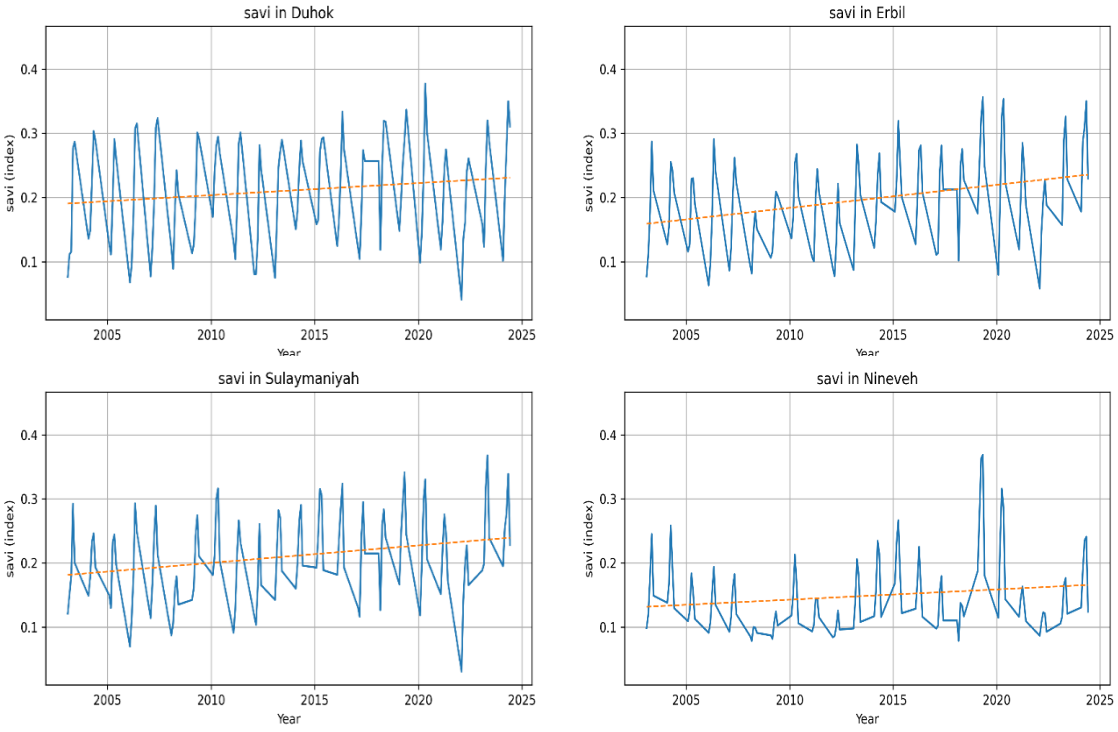

Figure 16: SAVI northern Iraqi regions during the period 2003 -2024.

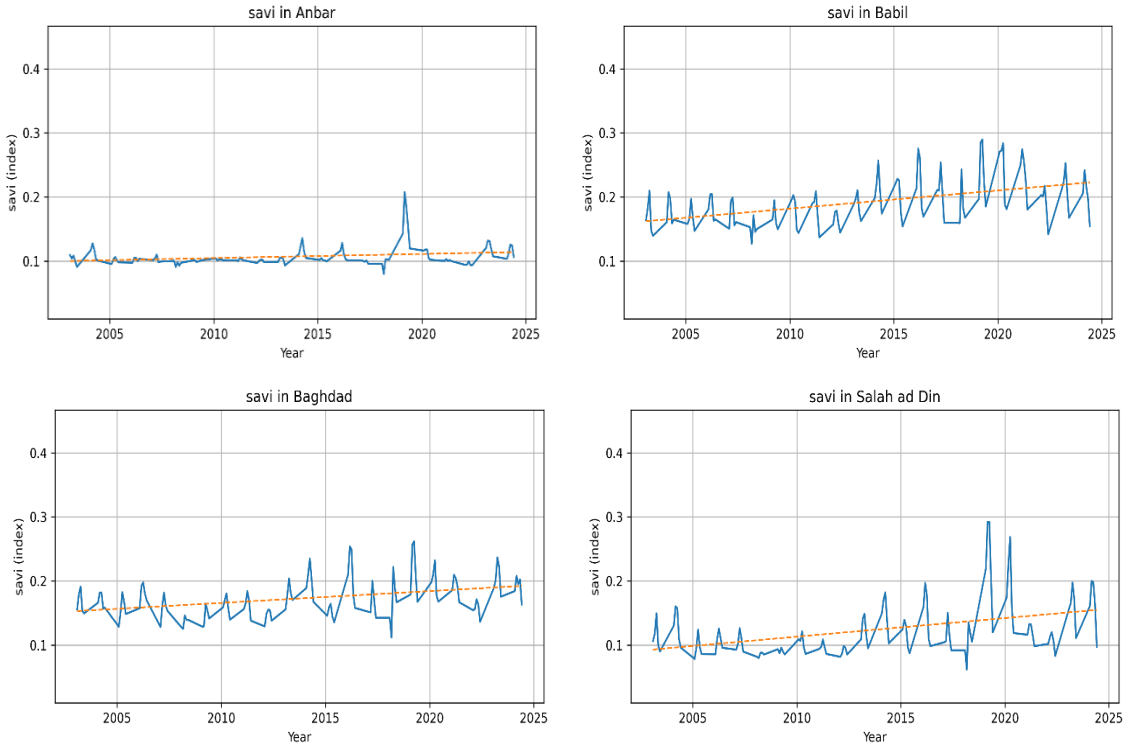

Figure 17: SAVI middle Iraqi regions during the period 2003 -2024.

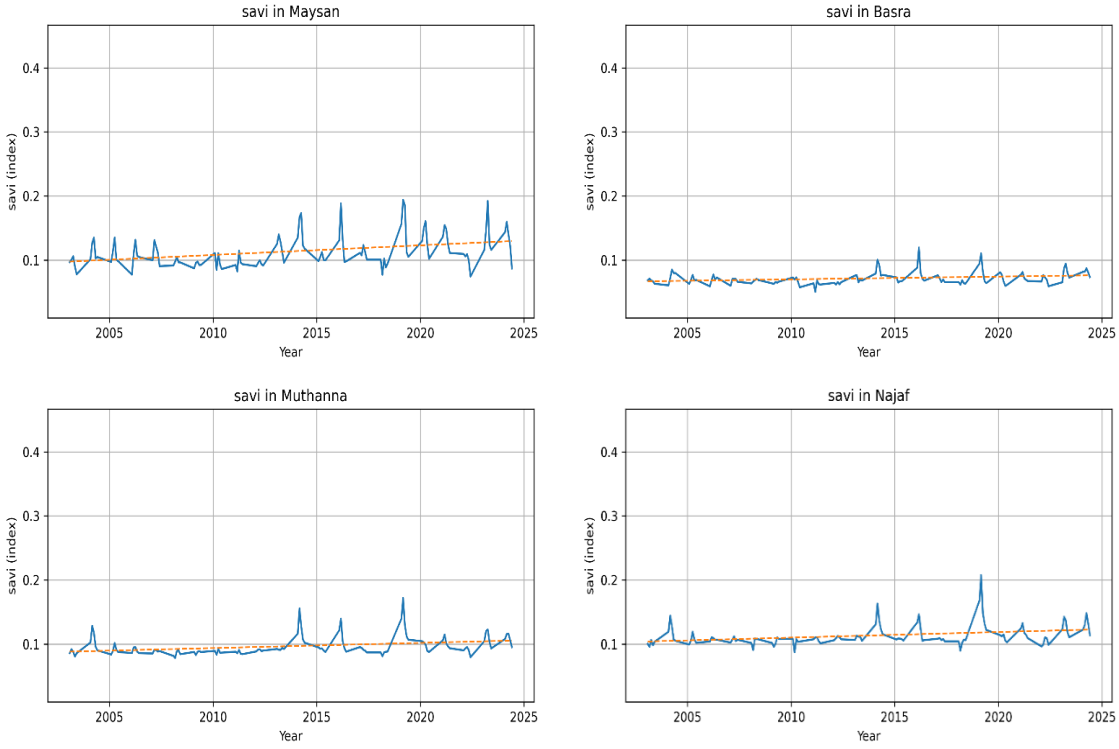

Figure 18: SAVI southern Iraqi regions during the period 2003 -2024.

5. Conclusions

The analysis results showed clear spatial and thematic variation in the temporal behavior of climatic, atmospheric, and vegetation variables in the Iraqi regions studied. The highest and most statistically significant warming rates were recorded in the middle and southern governorates, particularly Baghdad, Muthanna, and Najaf. In contrast, the northern governorates showed relatively weaker warming signals, reflecting a north-south gradient in thermal sensitivity. This suggests that middle and southern Iraq are more susceptible to prolonged heat stress, which could lead to increased evaporation rates, extreme heat effects, and more frequent droughts. Furthermore, CH_4 concentrations showed a strong, statistically significant upward trend across all regions and months, with particularly high rates of increase in the governorates of Nineveh, Anbar, and Muthanna. The rise in CH_4 concentrations is strongly associated with large-scale atmospheric processes rather than local factors. In contrast, CO shows a strong and statistically significant downward trend across all governorates, with the largest decreases recorded in northern and middle regions such as Nineveh, Sulaymaniyah, and Anbar. Carbon dioxide (CO_2), on the other hand, exhibits the most homogeneous behavior among all the studied variables, characterized by a strong, continuous, and statistically significant upward trend across all regions. The close convergence of Z and Q values confirms that the accumulation of CO_2 in the atmosphere over Iraq follows general global trends. Meanwhile, the SAVI index, which reflects vegetation dynamics, reveals significant spatial variation. Northern governorates, such as Erbil and Sulaymaniyah, show statistically significant positive trends, indicating relative resilience or improvement in vegetation cover. Conversely, governorates such as Nineveh, Anbar, and Basra record weak or negative trends, indicating drought and land degradation. Overall, the integrated results indicate that middle and southern Iraq are the most affected regions.

Conflict of Interest

The authors declare that they have no conflict of interest.

References

1. A. S. Abdulla, B. Al-Abudi, M. Mahdi, Classification of al-Hammar marshes satellite images in Iraq using artificial neural network based on coding representation, *J. Eng. Appl. Sci.* **14**(11)**,** 3651 (2019). https://doi.org/10.36478/jeasci.2019.3651.3658.
2. B. M. Hashim, A. Al Maliki, E. A. Alraheem, A. M. S. Al-Janabi, B. Halder, Z. M. Yaseen, Temperature and precipitation trend analysis of the Iraq Region under SRES scenarios during the twenty-first century, *Theor. Appl. Climatol.* **148,** 881 (2022). https://doi.org/10.1007/s00704-022-03976-y.
3. G. Ahmed, D. Al-Manmi, Trend detection of average annual rainfall and temperature in Sulaymaniyah Governorate, Iraq, *Anbar J. Agric. Sci.* **19**, 221 (2021). https://doi.org/10.32649/ajas.2021.175995.
4. F. Aswad, A. Yousif, S. Ibrahim, Trend analysis using Mann-Kendall and Sen's slope estimator test for annual and monthly rainfall for Sinjar District, Iraq, *J. Univ. Duhok* **32**, 501 (2020). https://doi.org/10.26682/csjuod.2020.23.2.41.
5. M. Q. Ali, Analysis of monthly temperature changes in Iraq to Duration (1950-2021), *Al-Adab J.* **152**(152), 289 (2025). https://doi.org/10.31973/jehd0609.
6. A. A. S. M. Mail, Seasonal and Annual Changes of Rainfall in Iraq During the Period from 1992 to 2010, *Alustath J. Hum. Soc. Sci.* **58(4)**, 25 (2019). https://doi.org/10.36473/ujhss.v1i7.944.
7. K. D. Muslih, K. Błażejczyk, Assessment of bioclimatic conditions and climate change in Iraq, *Theor. Appl. Climatol.* **130**, 583, (2017). https://doi.org/10.1007/s00704-016-1915-6.
8. M. Hamidi, A. Roshani, Investigation of climate change effects on Iraq dust activity using LSTM, *Atmos. Pollut. Res.* **14**, 1 (2023). https://doi.org/10.1016/j.apr.2023.101874.
9. Y. K. Al-Timimi, A. M. Al-Lami, F. S. Basheer, A. Y. Awad, Impacts of climate change on thermal bioclimatic indices over Iraq, *Iraqi J. Agric. Sci.* **55**(2), 744 (2024). https://doi.org/10.36103/j93nst49.
10. A. Allami, Z. Salih, R. Al-Bayati, A. Al-Salihi, A. Saleh, Some Comments on Air Pollution Levels over Iraq during Covid19 Pandemic Period Employing Remotely Sensed Data, *J. Res. Atmos. Sci.* **2**, 10 (2021). https://doi.org/10.29228/resatmsci.55066.
11. Z. Frayeh, N. Hamad, Estimating long-term trends in elements and some phenomena of Iraq's climate, *Dirasat Hum. Soc. Sci.* **51**, 33 (2024). https://doi.org/10.35516/hum.v51i1.10018.

12. D. A. Bilal, K. J. Al-Jumaily, E. A. Habbib, Air temperature trends in Baghdad, Iraq for the period 1941–2000, *Int. J. Sci. Res. Publ.* **3**, 1 (2013).
13. A. S. Hassan, J. H. Kadhum, Analysis the Intensity of CO_2 Emissions from Fossil Fuel Combustion in Iraq, *Al-Mustansiriyah J. Sci.* **32**(2)**,** 2 (2021). https://doi.org/10.23851/mjs.v32i2.982.
14. J. Rajab, A. Al-Salihi, Evaluation of the trends variance of atmospheric environment using MAKESENS model with spatiotemporal seasonal analysis over Iraq 2003–2021, *Afr. J. Biol. Sci.* **6**, 118 (2024). https://doi.org/10.33472/AFJBS.6.6.2024.118-133.
15. N. Al-Ansari, Topography and climate of Iraq, *J. Earth Sci. Geotech. Eng.* **11**, 1 (2021). https://doi.org/10.47260/jesge/1121.
16. H. B. Mann, Nonparametric tests against trend, *Econometrica.* **13**, 245 (1945). https://doi.org/10.2307/1907187.
17. R. M. Hirsch, J. R. Slack, R. A. Smith, Techniques of trend analysis for monthly water quality data, *Water Resour. Res.* **18**(1)**,** 107 (1982). https://doi.org/10.1029/WR018i001p00107.
18. A. R. Huete, A Soil-Adjusted Vegetation Index (SAVI), *Remote Sens. Environ.* **25**, 295 (1988). https://doi.org/10.1016/0034-4257(88)90106-X.
19. A. Bannari, D. Morin, F. Bonn, A. R. Huete, A Review of Vegetation Indices, *Remote Sens. Rev.* **13**, 95 (1995). https://doi.org/10.1080/02757259509532298.
20. J. L. Awange, J. B. Kiema, Fundamentals of GIS, *Environ. Geoinformatics* **13**, 191 (2013). https://doi.org/10.1007/978-3-642-34085-7_13.
21. J. Li, A. D. Heap, A Review of Spatial Interpolation Methods for Environmental Scientists, *Environ. Model. Softw.* **53**, 173 (2014). https://doi.org/10.1016/j.envsoft.2013.12.008.

تحليل الاتجاهات المناخية والبيئية في العراق باستخدام نهج متكامل يجمع بين نظم المعلومات الجغرافية واختبار مان-كيندال

أيمن موفق أحمد[2،1] وبشرى قاسم نقيب[1] وعلاء غضبان خلف[3]

[1]قسم الفلك والفضاء، كلية العلوم، جامعة بغداد، بغداد، العراق

[2]قسم التحسس النائي، كلية التحسس النائي والجيوفيزياء، جامعة الكرخ للعلوم، بغداد، العراق

[3]هيئة البحث العلمي، بغداد، العراق

الخلاصة

تتناول هذه الدراسة الاتجاهات المكانية والزمانية لمتغيرات مناخية وبيئية مختارة في مناطق مختلفة من العراق خلال الفترة من يناير إلى مايو من عام 2003 إلى عام 2024، وذلك باستخدام تقنيات نظم المعلومات الجغرافية (GIS) واختبار مان-كيندال للاتجاه. ويركز التحليل على خمسة متغيرات: درجة حرارة الهواء، والميثان، وأول أكسيد الكربون، وثاني أكسيد الكربون، ومؤشر الغطاء النباتي المعدل حسب التربة (SAVI). وقد جُمعت مجموعة بيانات شاملة من خلال دمج بيانات الأقمار الصناعية للمتغيرات المناخية والبيئية، وصور الاستشعار عن بُعد من جهاز MODIS لتقدير مؤشر SAVI، وبيانات درجة حرارة الهواء المرصودة من الهيئة العراقية للأرصاد الجوية وعلم الزلازل. وقُيّمت الاتجاهات الزمنية باستخدام اختبار مان-كيندال، وهو أسلوب لا معلمي للكشف عن التغيرات الرتيبة، بينما استُخدم مُقدِّر ميل ثيل-سين لتحديد معدل التغير بمرور الوقت. ولأغراض التحليل المكاني، صُنِّف العراق إلى ثلاث مناطق مناخية: الشمالية والوسطى والجنوبية. ساهم هذا التقسيم الإقليمي في تحديد أوضح للاختلافات المكانية والموسمية في المناخ والظروف البيئية. وكشفت النتائج عن تباينات إقليمية واضحة، حيث شهدت المحافظات الوسطى والجنوبية أعلى معدلات الاحترار، بينما أظهرت المناطق الشمالية تغيرات حرارية أقل حدة. وارتفع غاز الميثان بشكل ملحوظ في جميع المناطق، في حين انخفض ثاني أكسيد الكربون بشكل ملحوظ. وشهد ثاني أكسيد الكربون اتجاهًا تصاعديًا ثابتًا على مستوى البلاد. وتفاوتت اتجاهات مؤشر الغطاء النباتي (SAVI) بين المناطق، حيث أظهرت المحافظات الشمالية استجابات نباتية إيجابية، بينما شهدت المناطق الجنوبية والغربية ركودًا أو تدهورًا. وبشكل عام، يواجه وسط وجنوب العراق أكبر قدر من الضغوط البيئية، نتيجة لتسارع الاحترار، وارتفاع انبعاثات غازات الاحتباس الحراري، وضعف قدرة الغطاء النباتي على الصمود، مما يسلط الضوء على الحاجة المُلحة إلى استراتيجيات تكيف مُوجهة وإدارة مستدامة للأراضي.

الكلمات المفتاحية: العراق، مؤشر SAVI، نظم المعلومات الجغرافية (GIS)، المناخ، الميثان.